RSC Advances

PAPER

View Article Online
View Journal | View Issue

Cite this: *RSC Adv.*, 2021, **11**, 4983

Immunoassay-aptasensor for the determination of tumor-derived exosomes based on the combination of magnetic nanoparticles and hybridization chain reaction†

Hua Zhang,‡[a] Yajuan Zhou,‡[b] Dan Luo,[a] Jingjian Liu,[a] E. Yang,[c] Guangyi Yang,[c] Guangjun Feng,[c] Qinhua Chen *[c] and Lun Wu*[a]

Received 2nd December 2020
Accepted 10th January 2021

DOI: 10.1039/d0ra10159a

rsc.li/rsc-advances

The detection of tumor-related exosomes is of great significance. In this work, a fluorescence aptasensor was designed for the determination of tumor-related exosomes based on the capture of magnetic nanoparticles (MNPs) and specific recognition of an aptamer. MNPs were used as substrates to capture the exosomes by modifying the CD63 antibody on the MNP surface. Probe 1 consists of PDL-1 aptamer sequence and a section of other sequences. PDL-1 expression was observed on the surface of exosomes; the aptamer of PDL-1 could combine with PDL-1 with high affinity. Thus, the immunoassay-type compounds of "MNPs–exosomes–probe 1" were formed. The other section of probe 1 triggered the HCR with probe 2 and probe 3 and formed the super-long dsDNA. The addition of GelRed resulted in the generation of an amplified fluorescence signal. The proposed design demonstrated a good linearity with the exosome concentration ranging from 300 to 10^7 particles per mL and with a low detection limit of 100 particles per mL. This aptasensor also exhibited high specificity for tumor-related exosomes, and was successfully applied in biological samples.

1. Introduction

The worldwide morbidity and mortality of cancer are increasing every year. Cancer is a serious threat to human life and health.[1] Tumor markers play an important role in the early diagnosis and treatment of cancers.[2] As effective cancer monitors, exosomes have shown promising advantages in liquid biopsies because of their noninvasive measurement and predictability of the disease.[3] Exosomes are membrane-coated extracellular vesicles with a diameter of about 30–200 nm,[4] and are secreted by many types of eukaryotic cells into the extracellular space.[5] They are detectable in various bodily fluids, including blood, urine, saliva, breast milk and amniotic fluid.[6] Exosomes carry large amounts of proteins, lipids, DNA, RNA, and other biological molecules, which can provide information about the originating tumor.[7] For tumors, especially for malignant tumors, exosomes participate in the composition and regulation of the local microenvironment, which affect the growth and development of the tumor.[8] Tumor-derived exosomes play crucial roles in cancer occurrence and progression.[9] They have been recognized as promising biomarkers for an early noninvasive diagnosis of cancers.[10]

However, the small size and low buoyant density of exosomes pose significant challenges for their separation and quantification from the complex biological fluids.[11] At present, the recognized standard methods widely used for exosome quantification and analysis include transmission electron microscopy (TEM), dynamic light scattering (DLS), nanoparticle tracking analysis (NTA), atomic force microscopy (AFM), western blot (WB), enzyme-linked immunosorbent assay (ELISA), tunable resistive pulse sensing (RPS), flow cytometry and mass spectrometry (MS).[11–14] All of the aforementioned methods are used to analyze one characteristic aspect of exosomes, *e.g.* TEM is usually used to characterize the morphological characteristics, DLS and NTA are used to analyse the size and concentration of exosomes. WB and ELISA are the methods used to analyze the marker proteins of exosomes.[15] However, there are several drawbacks that limit the application scope of the above methods. First, all of the above-mentioned methods require state-of-the-art instruments, and these instruments are very expensive and thus increase the cost. Second, the selectivity for some specific exosomes is poor. Most importantly, the accuracy of exosome determination is affected by unknowable

[a]*Affiliated Dongfeng Hospital, Hubei University of Medicine, Shiyan, 442008, Hubei, China. E-mail: wulun0909@163.com*

[b]*Department of Radiotherapy, Hubei Cancer Hospital, Tongji Medical College, Huazhong University of Science and Technology, Wuhan, 430074, China*

[c]*Shenzhen Baoan Authentic TCM Therapy Hospital, Shenzhen, Guangdong, 518101, China. E-mail: cqh77@163.com; Tel: + 86-0719-8272238*

† Electronic supplementary information (ESI) available. See DOI: 10.1039/d0ra10159a

‡ Hua Zhang and Yajuan Zhou are the Co-first authors.

nanoparticle counting, which formed by proteins aggregate and lipoprotein particles, and even some exosomes less than a certain size being ignored.[12] Fortunately, with in-depth research, some advanced technologies with recognition element for exosome assay have been developed.

Recently, considering the importance of exosomes in the liquid biopsy of cancer, many studies have explored new detection techniques over the past few decades.[16] A series of novel technologies have been developed for the determination of exosomes, including fluorescence detection,[17] electrochemical biosensors,[5,14,18,19] immunosensors,[13,20] surface plasmon resonance (SPR),[21–23] microfluidic devices,[21] electrochemiluminescence,[24] aptasensors,[25] and spectroscopic analysis.[26] However, these established exosome assays usually involve labour-intensive steps and require extended quantitative protocols and expensive laboratory infrastructures. They suffer from low sensitivity and high-cost and thus are impractical for wide use. In addition, most of these strategies are unable to distinguish cancer cell-derived exosomes from the normal exosomes, which limits their application in clinical cancer diagnosis. Based on this, we designed a novel biosensor that could with high specificity determine the concentration of tumor-related exosomes by measuring the fluorescence intensity, which combined GelRed with magnetic nanoparticles (MNPs).

In this design, aptamer plays an extremely important role. Aptamers are single-stranded oligonucleotides folding into specific tertiary structures, which bind to their molecular targets, including small molecules, peptides, proteins and cells with high specificity and affinity.[27,28] Aptamers have been termed "chemical antibodies" and predicted to replace antibodies in the near future.[29] Therefore, the aptamer of PDL-1 can bind with PDL-1 specifically in this research. For signal amplification, hybridization chain reaction (HCR) is one of the most popular techniques to improve the detection sensitivity.[30] Thus, this signal amplification method can significantly improve the sensitivity for the determination of tumor-related exosomes. In this work, we used the exosomes triggering the HCR and obtained the super-long dsDNA. The GelRed, being a stable, sensitive and environmentally friendly fluorescent nucleic acid staining dye,[31,32] could chimerize into the dsDNA structure and generate a strong fluorescence signal.[33] Thus, we could realize the detection of tumor-related exosomes by measuring the final fluorescence signal.

2. Material and methods

2.1 Reagents

All synthetic DNA sequences and aptamer were purchased from Sangon Biotechnology Co. Ltd. (Shanghai, China) and are listed in Table 1. 10% fetal bovine serum was purchased from Sigma-Aldrich (St. Louis, MO, USA). Anti-CD63 antibody was purchased from Abcam (Cambridge, MA, UK), and carboxylated MNPs were bought from XFNANO Co., Ltd. (Nanjing, China). The GelRed (1 × 10 000) was bought from Solarbio (Beijing, China). A549 non-small cell lung cancer (NSCLC) cells and BEAS-2B normal human bronchial epithelial cells were obtained from Procell (Wuhan, China). Ultrapure water prepared from a Millipore water purification system (a resistivity of 18 MΩ cm, Milli-Q Direct 8) was used in all the runs.

2.2 Cell culture

All cell culture media were supplemented with 10% fetal bovine serum, 1% 100 U mL^{-1} penicillin, and 100 μg mL^{-1} streptomycin at 37 °C in a humidified 5% CO_2 incubator. The conditioned medium was collected after 48 h following serum-free defined medium. Exosomes were isolated using the standard ultracentrifugation method with slight modifications. A549 non-small cell lung cancer (NSCLC) cells and BEAS-2B normal human bronchial epithelial cells were cultured in RPMI 1640 and DMEM, respectively, with 10% FBS, at 5% CO_2 in culture bottles.

2.3 Extraction of exosomes

The supernatant was collected from the conditioned medium after A549 and BEAS-2B cells were cultured in a serum-free defined medium for 48 h. Then, standard ultracentrifugation with slight modifications was employed to extract exosomes from the supernatant. First, the medium was centrifuged at 300*g* at 4 °C for 10 min to remove the residual cells. Second, the cell debris and apoptotic vesicles were removed by centrifugation at 2000*g* for 20 min. The supernatant was collected and filtered through a filter with a pore size of 0.22 μm (Millipore).

Table 1 All of the synthetic DNA sequences and aptamer of PDL-1 used in this sensor

Name	Sequences
Aptamer of PDL-1	5′-ACG GGC CAC ATC AAC TCA TTG ATA GAC AAT GCG TCC ACT GCC CGT-3′
Probe 1	5′-AGC TTT AAT TAA CAT GTC CGA CTTT ACG GGC CAC ATC AAC TCA TTG ATA GAC AAT GCG TCC ACT GCC CGT-3′
Probe 2	5′-GTC GGA CAT GTT AAT TAA AGC TTA GCA TCG ACT AGC TTT AAT TA-3′
Probe 3	5′-AGC TTT AAT TAA CAT GTC CGA CTA ATT AAA GCT AGT CGA TGC TA-3′
Probe 4	5′-AGC TTT AAT TAA CAT GTC CGA C ATC ATC GTA TTA CCG AAC TCG GTA CAT-3′

The filtrate was further centrifuged at 10 000*g* for 30 min to remove the cell vesicles and biological macromolecules. Subsequently, the supernatant was centrifuged at 100 000*g* at 4 °C for 70 min, and the sediment was resuspended in 20 mL sterile phosphate-buffered saline (PBS). Then, the resuspension was pelleted again by ultracentrifugation for 2 h at 100 000*g* at 4 °C. Finally, the supernatant was discarded, and exosomes were obtained as residual sediments. The extracted exosomes were resuspended in 200 μL PBS and was ready for use.

2.4 Characterization of exosomes

2.4.1 TEM. The morphological characteristics of the extracted exosomes were analyzed by transmission electron microscopy (TEM). The carbon-coated copper 400 mesh was floated on top of a 20 μL droplet of exosome suspension for 5 min (carbon side down). The samples were then fixed on the copper grid with 2% glutaraldehyde (Sigma-Aldrich) for 20 minutes, and then dried at room temperature. Then, the grids were dipped and dyed in 2% phosphotungstic acid. Images of the exosomes were obtained *via* a transmission electron microscope (TEM) (Hitachi H-7000 NAR) operating at 80 kV soon after the samples were washed with PBS and dried at room temperature.

2.4.2 NTA. The concentration and size distribution of the exosomes could be analyzed by nanoparticle tracking analysis (NTA). The suspensions were diluted in PBS until an optimal particle concentration of 1/50 was obtained after filtering through a 0.22 μm pore filter. After that, the samples were injected into the equipment and illuminated by the NTA laser beam. The typical Brownian motion of exosomes could scatter lights and be observed by a microscope equipped with a 405 nm laser and sCMOS camera (ZetaView Ltd., Germany). Under the optimal settings, the individual exosomes in the suspensions could be visualized. All tests were performed at room temperature. Each sample was tested 3 times.

2.5 Fluorescent aptasensor construction and exosome determination

The strategy of exosome determination was carried out by following the procedure below: the carboxylated MNPs (20 μg mL^{-1}) were activated with a mixture of 200 mM EDC and 50 mM NHS for 30 min. The anti-CD63 antibody (10 μg mL^{-1}) was modified on the above prepared MNPs for 2 h. Then, the MNPs were blocked with BSA solution (100 μg mL^{-1}) for 2 h. Consecutively, 100 μL of NTA-calibrated exosome solution was added and incubated at 37 °C for 30 min. The marker protein CD63 on the exosome surface can specifically bind to the CD63 antibody on the surface of the MNPs, which made the MNPs capture the exosomes. Then, 20 nM probe 1 was added and incubated for 30 min. Probe 1 (DNA sequence) consisting of an aptamer of PDL-1 and an initiator of HCR can bind to exosomes and form the complex of "MNPs–exosomes–probe 1". A mixture of probe 2 (40 nM) and probe 3 (40 nM) strands was heated at 95 °C for 5 min, followed by slow cooling to room temperature. Then, the mixture was incubated with the above obtained MNPs for 30 min at 37 °C. Probe 2 and probe 3 hybridized with the HCR initiator and extended the hybridization chain. Then, GelRed (1 × 600) was added to the mixture. All reaction solutions were PBS solution and the volume was 1 mL. The modified MNPs were obtained through magnetic separation in each step and washed with PBS for 3 times. The content of exosomes was determined by detecting the final fluorescence intensity.

2.6 Fluorescence measurements

The fluorescence measurement was carried out at room temperature on a Hitachi F-4600 spectrophotometer (Hitachi Co. Ltd., Japan, https://www.hitachi.co.jp) equipped with a xenon lamp as the excitation source. The excitation wavelength was set at 518 nm. The fluorescence spectra were collected at an emission wavelength of 580–750 nm. The optimum experimental parameters were studied by using the fluorescence intensity at 606 nm. The performance of this designed detection system was also evaluated. The excitation and emission intervals were both set at 5 nm. Except for the special groups, the fluorescence intensity of each group was measured three times and the standard deviation was calculated. The quantitative determination of exosomes was expressed by the final fluorescence intensity.

2.7 Application in clinical blood samples

The blood samples collected from 8 normal human subjects and 8 lung cancer patients were added with an appropriate amount of thrombin and were centrifuged at 3000*g* at 4 °C for 5 min. Afterward, the supernatant samples were further filtered through a 0.8 μm pore filter. Finally, the exosomes were collected by centrifuging the obtained filtrate at 100 000*g* at 4 °C for 60 min. All experiments in this study were conducted in strict accordance with the institutional regulations and relevant laws (National Health Commission of the People's Republic of China, Ethical Review of Biomedical Research Involving Human Beings). The plasma of patients with lung cancer and the healthy human plasma were acquired from Affiliated Dongfeng General Hospital, Hubei University of Medicine. This study was approved by the Dongfeng General Hospital's Ethics Committee (Shiyan, China). Informed consent was obtained for any experiment performed on patients with lung cancer and healthy human subjects.

3. Results and discussion

3.1 Principle of exosome determination

As shown in Fig. 1, the determination mechanism of exosome is based on the recognition of the antibodies and the specific binding of aptamers to the target. CD63 is the marker protein expressed on the surface of exosomes.[34] The surface of the carboxylated MNP was modified with CD63 antibody, which could capture exosomes specifically. PDL-1 was expressed on the surface of the tumor-related exosomes,[35,36] so that probe 1 (consisting of aptamer of PDL-1 and initiator of HCR) could bind with the complexes of "MNPs–exosomes" and form "MNPs–exosomes–probe 1". With the addition of probe 2 and probe 3, the initiator of HCR could bind with probe 3 and made

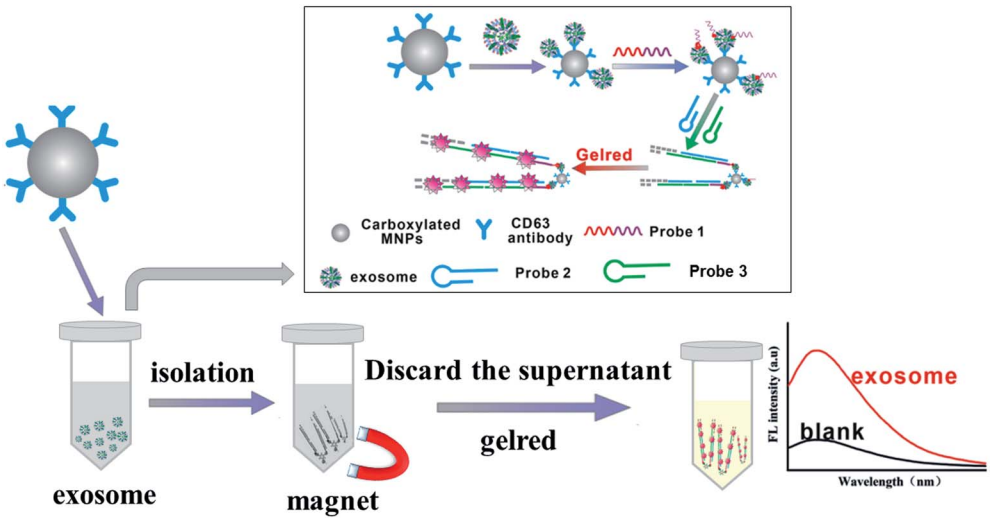

Fig. 1 Schematic illustration of the immunoassay-aptasensor for exosome detection based on the combination of MNPs and HCR.

the HCR occur in probe 2. With the addition of GelRed and the extension of probe 2/probe 3 hybrid duplex, GelRed formed a soluble complex with nucleic acids and generated fluorescence signals. Thus, the concentration of the tumor-associated exosome could be quantified specifically by the measurement of the final fluorescence intensity.

3.2 Characterization of exosomes

NSCLC-specific exosomes were isolated from the culture medium of A549 NSCLC cell lines by ultracentrifugation. In order to confirm the successful extraction of exosomes, the morphology of the exosomes was observed by using TEM. In addition, the concentration and size distribution of the exosome were analyzed by NTA. As shown in Fig. 2a, we can clearly see the presence of exosomes with different sizes, and the average diameter is about 150 nm in TEM. The concentration and diameter of the extracted exosomes can be seen in Fig. 2b. The exosomes were resuspended in PBS and the mother liquor was diluted for 50 times. The detecting concentration of exosomes was 3.7×10^8 particles per mL, and the actual concentration of exosomes was about 1.85×10^{10} particles per mL with a size distribution of 50 to 200 nm. The above characterization results showed that a large amount of exosomes with narrow and uniform size had been extracted successfully.

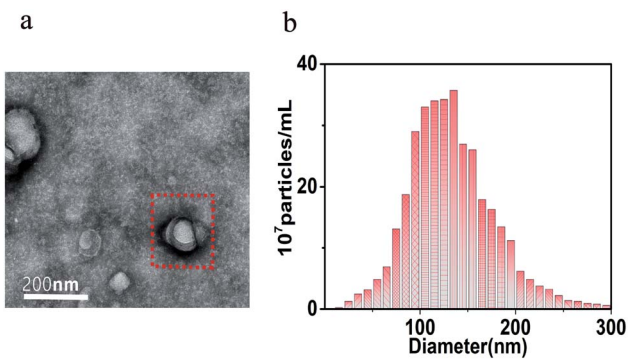

Fig. 2 Characterization of exosomes. (a) The TEM image of exosomes and (b) the NTA analysis of exosomes.

3.3 Experimental condition optimization

During the experimental process, there were five parameters that affected the sensing efficiency. In order to obtain the ideal performance for the determination of exosomes, these conditions were optimized: (a) the concentration of MNPs, (b) the concentration of CD63 antibody, (c) the concentration of probe 1, (d) the concentration of probe 2, and (e) the reaction time of HCR.

It was worth noting that as the substrate for capturing exosomes, the concentration of MNPs affects the efficiency of exosome determination. Under different concentrations of MNPs, there were several changes in the final fluorescence intensities. Fig. 3a shows that the fluorescence signal changes with an increase in the concentration of MNPs from 5 to 40 μg mL^{-1}. The fluorescence signal stabilized when the concentration of MNPs was 20 μg mL^{-1}. We chose the point where the fluorescence intensity became stable as the optimal concentration. MNPs were utilized as the substrate to capture exosomes. The exosomes would aggregate at a high concentration of MNPs. Moreover, at low concentrations of MNPs, less exosomes were captured. About 20 μg mL^{-1} was found to be the optimum concentration of MNPs. The concentration of CD63 antibody played a significant role in the sensing performance of this sensor. The concentration of CD63 antibody affected the formation of the antibody modified MNPs and whether this method can detect exosomes. The results shown in Fig. 3b display significant changes in the fluorescence intensities at a series of CD63 antibody concentrations. The relatively steady fluorescence intensity was observed when the concentration of CD63 antibody was 10 μg mL^{-1}. When the concentration of CD63 antibody was decreased gradually, the fluorescence intensity decreased dramatically. Furthermore, when the

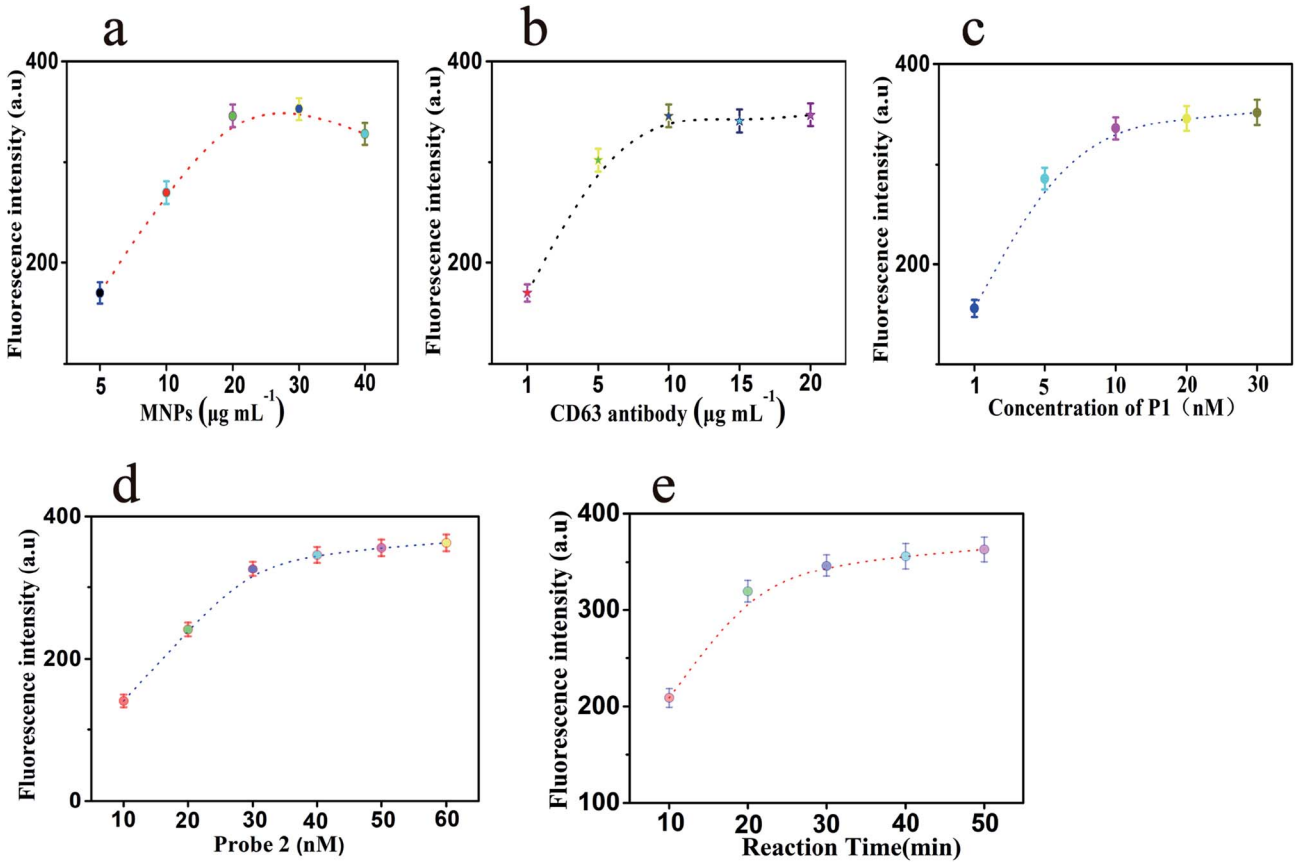

Fig. 3 Effects of the reaction parameters on the fluorescence signals of the proposed method: (a) the concentration of MNPs (μg mL^{-1}), (b) the concentration of CD63 antibody (μg mL^{-1}), (c) the concentration of P1 (nm), (d) the concentration of probe 2 (nm) and (e) reaction time (min).The lines represent the fluorescence intensity at different conditions. Error bars: SD, $n = 3$.

concentration of CD63 antibody was increased to 15 μg mL^{-1}, the change in fluorescence was almost negligible and tended to be stable. Therefore, the optimal concentration of CD63 antibody was 10 μg mL^{-1}, which could be used in the subsequent experiments.

At the same time, the concentration of probe 1 would affect the connection between the MNPs and the exosomes. It would also affect whether this method can detect tumor-related exosomes. Thus, we chose different concentrations of probe 1 to optimize. Fig. 3c shows the results. With an increase in the concentration of probe 1 from 1 to 30 nM, the fluorescence intensity increased gradually and then tended to be steady. The changes in the fluorescence intensity with respect to the concentration of probe 1 at 20 nM could be neglected. A relatively stable fluorescence intensity was observed when the concentration of probe 1 was 20 nM. Therefore, 20 nM was considered as the best concentration of probe 1. The concentration of probe 2 affects the formation and extension of the hybrid duplexes (probe 2/probe 3) and further affects the dyeing efficacy of GelRed with probe 2/probe 3 to generate fluorescence signals. As shown in Fig. 3d, with an increase in the concentration of probe 2 from 10 to60 nM, the fluorescence intensity increases gradually and tends to be stable. When the concentration of probe 2 was 40 nM, the fluorescence intensity reached a relatively stable state. When the concentration was increased to 50 nM or 60 nM, there was a slight change in fluorescence. To obtain a better performance, we chose 40 nM as the optimal concentration.

Finally, the reaction time of HCR was another significant parameter that affected the fluorescence intensity. As shown in Fig. 3e, with an increase in the reaction time, the fluorescence intensity increases first and then becomes steady. A relatively stable fluorescence intensity was observed when the reaction time was 30 min. After 30 minutes, the signal continued to increase when prolonging the reaction time. However, with the extension of reaction time, the background signal will also increase. An increase in the background signal was not conducive to reducing the minimum detection limit of the method. Considering the influence, when the reaction time was 30 min, better experimental results could be obtained in a shorter time. On the other hand, MNPs will be inactivated if the reaction time was too long. In addition, the shorter reaction time will lead to an incomplete dyeing of GelRed and probe 2/probe 3 duplexes. Therefore, the reaction time of 30 min was regarded as the optimum reaction time for the rest of the experiments.

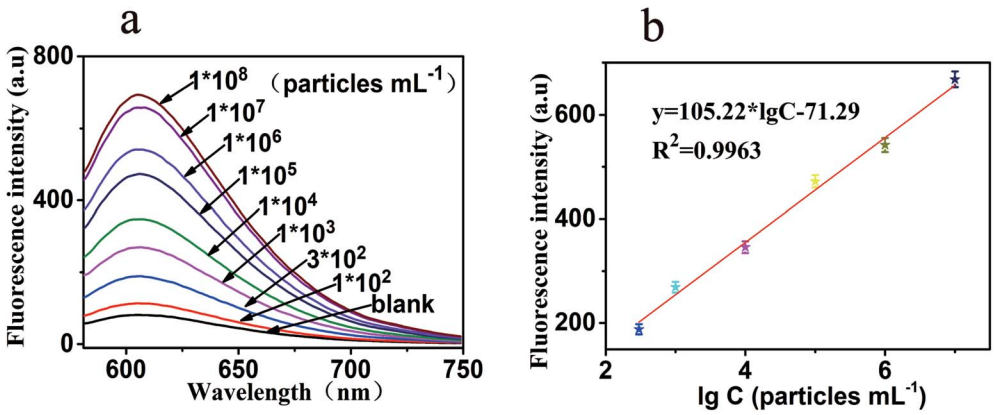

Fig. 4 (a) Fluorescence emission spectra of the biosensor in the presence of exosomes with different concentrations: from bottom to top: 0 to 1 × 10^8 particles per mL, (b) the fluorescence intensity as a function of exosome concentration. It shows a strong correlation between the fluorescence intensity and the exosome concentration and the emission wavelength of 606 nm. Error bars: SD, $n = 3$.

3.4 Analytical performance

Under the above optimal parameters, the analytical performance of this sensor was evaluated at different concentrations of exosomes. Each experiment was repeated three times, and the result was the mean value of three measurements. There were numerous PDL-1 on the surface of the exosomes, and one exosome can combine with multiple probe 1 to form the 1:N signal amplification mode. Secondly, one probe 1 can also induce HCR to obtain a super long double-stranded DNA, which formed exponential amplification of the signal. Therefore, an increase in the concentration of exosomes could increase the signal exponentially. As shown in Fig. 4a, of the 9 different samples we tested, 6 samples show a linear relationship. The fluorescence intensity increased gradually as the concentration of exosomes was increased from 0 to 1 × 10^8 particles per mL. Furthermore, a good linearity between the fluorescence intensity and the logarithm to the base 10 of exosome concentration was observed. The linear regression equation was $y = 105.22 \times \lg C - 71.29$ ($R^2 = 0.9963$), where y and lg C, respectively, represented the fluorescence intensity and the logarithm of exosome concentration. These data can be seen in Fig. 4b. The detection limit of this method for exosome determination was calculated to be as low as 100 particles per mL, and the linear range was 300 to 10^7 particles per mL. As shown in Table 2, the analytical performance of this strategy was compared with the other recently reported literature.

In order to verify the specificity of this biosensor for exosome determination, control experiments were carried out by using cTnI, probe 4, normal cells and the blank group. We used cTnI instead of CD63 to modify MNPs, probe 4 instead of probe 1, and the BEAS-2B normal human bronchial epithelial cells replaced A549 NSCLC cells; results are shown in Fig. 5. Testing these five different groups under the same conditions exhibited the specificity of this method for exosome determination. Compared with the blank group, there were weak and negligible fluorescence peaks observed in the other three groups (including cTnI, probe 4, and normal cells). In the experimental group of exosomes from A549 NSCLC cells, there was a strong and obvious fluorescence peak. All of these results suggested that this sensor could only achieve the specific determination of tumor-related exosomes, and neither exosomes secreted by the normal cells nor other reagents replacing the originals. The

Table 2 The comparison between our method and other reported biosensors for the detection of exosomes

Analytical method	Detection limit	Linear range	Ref.
Fluorescence detection	3.12 × 10^3 particles per μL	1.0 × 10^4 to 5.0 × 10^5 particles per μL	12
Fluorescence detection	1.0 × 10^5 particles per μL	1.0 × 10^5 to 1.0 × 10^9 particles per μL	17
Electrochemical biosensor	1.72 × 10^4 particles per mL	1.0 × 10^5 to 5.0 × 10^7particles per mL	5
Electrochemical biosensor	7.83 × 10^3 particles per μL	9.5 × 10^3 to 1.9 × 10^7 particles per μL	14
Electrochemical biosensor	1.44 × 10^3 particles per mL	2.38 × 10^4 to 2.38 × 10^9 particles per mL	19
Immunosensor	1.4 × 10^8 particles per mL	—	13
Immunosensor	96 particles per μL	1.12 × 10^2 to 1.12 × 10^8 particles per μL	20
Surface plasmon resonance	3.86 × 10^8 particles per mL	—	21
Surface plasmon resonance	5 × 10^3particles per mL	—	23
Microfluidic devices	2.18 × 10^9 particles per mL	—	21
Electrochemiluminescence	37.0 particles per μL	1.1 × 10^2 to 1.1 × 10^7 particles per μL	24
Aptasensor	3.94 × 10^5 particles per mL	8.3 × 10^5 to 5.3 × 10^7 particles per mL	25
Immunoassay-aptasensor	100 particles per mL	300 to 10^7 particles per mL	This sensor

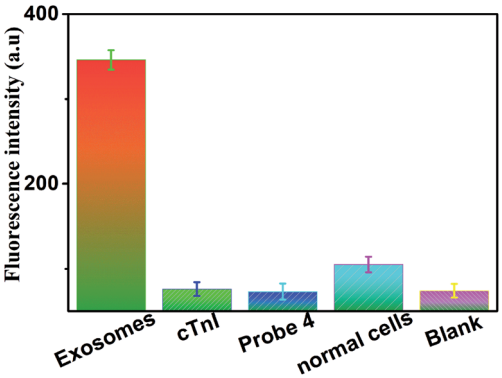

Fig. 5 Fluorescence intensity (at an emission wavelength of 606 nm) of the sensor in the presence of exosomes, cTnI, probe 4, normal cells and blank, respectively. Error bars: SD, $n = 3$.

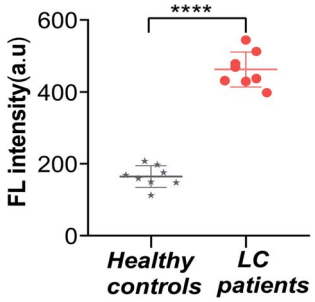

Fig. 6 Fluorescence intensity of the sensor for the detection of exosomes from LC patients and healthy controls (****$P < 0.0001$). Error bars: SD, $n = 3$.

excellent specificity of our strategy was mainly attributed to the high affinity and specific recognition between the aptamers (or antibodies) and the targets.

3.5 Application in biological samples

In order to investigate the feasibility and practical application of this sensor in real biological samples, we obtained plasma from patients with lung cancer (LC) and healthy human subjects. We extracted exosomes from 8 normal human subject plasma and 8 LC patient plasma; other conditions remained identical. The exosomes of the two groups were treated as described previously, added into the mixtures and measured the final fluorescence intensity. The results are shown in Fig. 6, and the fluorescence intensities of the samples from LC patients are stronger than that of the group of healthy human subjects. Furthermore, the difference in the fluorescence intensity between the two groups was statistically significant ($P < 0.0001$). These results indicated that the sensor could be applied for the analysis of exosomes from biological samples.

4. Conclusion

A fluorescent aptasensor was developed for the determination of exosomes. Based on the specific recognition of immunoassay, high specificity and sensitivity, the determination of LC-related exosomes was completed with a wide linearity range (300 to 10^7 particles per mL) and a low detection limit of 100 particles per mL. The proposed immunoassay-aptasensor could also be applied for the analysis of clinical samples, which has a practical application value and potential significance. Considering the wide presence of exosomes in types of tumor-derived biological fluids, by binding with the different aptamers of exosome marker protein, this strategy has broad application prospects in early diagnosis, treatment evaluation, as well as monitoring and prognosis of various cancers.

Conflicts of interest

There are no conflicts to declare.

Acknowledgements

These works were supported by the National Natural Science Foundation of China (81872509 and 81803065), the Hubei Province Health and Family Planning Scientific Research Project (WJ2019M054), 2020 Baoan District Medical and Health Basic Research Project (2020JD491 and 2020JD072), Bao'an TCM Development Foundation (2020KJCX-KTYJ-200), and the Internal Research Project of Shenzhen Baoan Authentic TCM Therapy Hospital (BCZY2021003).

References

1 J. Tang, Y. Wang, Y. Luo, J. Fu, Y. Zhang, Y. Li, Z. Xiao, Y. Lou, Y. Qiu and F. Zhu, *Comput. Struct. Biotechnol. J.*, 2020, **18**, 2012–2025.
2 A. Bobrie and C. Théry, *Biochem. Soc. Trans.*, 2013, **41**, 263–267.
3 M. L. Gao, F. He, B. C. Yin and B. C. Ye, *Analyst*, 2019, **144**, 1995–2002.
4 K. Kalimuthu, W. Y. Kwon and K. S. Park, *J. Biol. Eng.*, 2019, **13**, 31–38.
5 Y. Cao, L. Li, B. Han, Y. Wang, Y. Dai and J. Zhao, *Biosens. Bioelectron.*, 2019, **141**, 111397.
6 H. Zhang, B. Qiao, Q. Guo, J. Jiang, C. Cai and J. Shen, *Analyst*, 2020, **145**, 3557–3563.
7 L. Huang, D. Wang, N. Singh, F. Yang, N. Gu and X. Zhang, *Nanoscale*, 2018, **10**, 20289–20295.
8 C. Wang, D. Jin, Y. Yu, L. Tang, Y. Sun, Z. Sun and G. Zhang, *Sens. Actuators, B*, 2020, **314**, 128056.
9 R. Huang, L. He, Y. Xia, H. Xu, C. Liu, H. Xie, S. Wang, L. Peng, Y. Liu, Y. Liu, N. He and Z. Li, *Small*, 2019, **15**, e1900735.
10 Z. Yan, S. Dutta, Z. Liu, X. Yu, N. Mesgarzadeh, F. Ji, G. Bitan and Y. Xie, *ACS Sens.*, 2019, **4**, 488–497.
11 H. Xu, C. Liao, P. Zuo, Z. Liu and B. Ye, *Anal. Chem.*, 2018, **90**, 13451–13458.
12 Y. Xia, T. Chen, G. Chen, Y. Weng, L. Zeng, Y. Liao, W. Chen, J. Lan, J. Zhang and J. Chen, *Talanta*, 2020, **214**, 120851.
13 J. Suthar, E. S. Parsons, B. W. Hoogenboom, G. R. Williams and S. Guldin, *Anal. Chem.*, 2020, **92**, 4082–4093.

14 Z. Sun, L. Wang, S. Wu, Y. Pan, Y. Dong, S. Zhu, J. Yang, Y. Yin and G. Li, *Anal. Chem.*, 2020, **92**, 3819–3826.
15 Y. Sun, H. Jin, X. Jiang and R. Gui, *Anal. Chem.*, 2020, **92**, 2866–2875.
16 R. Huang, L. He, S. Li, H. Liu, L. Jin, Z. Chen, Y. Zhao, Z. Li, Y. Deng and N. He, *Nanoscale*, 2020, **12**, 2445–2451.
17 X. Yu, L. He, M. Pentok, H. Yang, Y. Yang, Z. Li, N. He, Y. Deng, S. Li, T. Liu, X. Chen and H. Luo, *Nanoscale*, 2019, **11**, 15589–15595.
18 L. Luo, L. Wang, L. Zeng, Y. Wang, Y. Weng, Y. Liao, T. Chen, Y. Xia, J. Zhang and J. Chen, *Talanta*, 2020, **207**, 120298.
19 Y. Zhu, Y. An, R. Li, F. Zhang, Q. Wang and P. He, *J. Electroanal. Chem.*, 2020, **862**, 113969.
20 K. H. Kholafazad and M. Hasanzadeh, *Anal. Methods*, 2020, **12**, 2795–2811.
21 M. Gaillard, A. Thuaire, G. Nonglaton, V. Agache, Y. Roupioz and C. Raillon, *Analyst*, 2020, **145**, 1997–2013.
22 G. Qiu, A. Thakur, C. Xu, S. Ng, Y. Lee and C. L. Wu, *Adv. Funct. Mater.*, 2019, **29**, 1806761.
23 Q. Wang, L. Zou, X. Yang, X. Liu, W. Nie, Y. Zheng, Q. Cheng and K. Wang, *Biosens. Bioelectron.*, 2019, **135**, 129–136.
24 D. Fang, D. Zhao, S. Zhang, Y. Huang, H. Dai and Y. Lin, *Sens. Actuators, B*, 2020, **305**, 127544.
25 Y. Zhou, H. Xu, H. Wang and B. C. Ye, *Analyst*, 2019, **145**, 107–114.
26 H. Shin, S. Oh, S. Hong, M. Kang, D. Kang, Y. Ji, B. H. Choi, K. Kang, H. Jeong, Y. Park, S. Hong, H. K. Kim and Y. Choi, *ACS Nano*, 2020, **14**, 5435–5444.
27 L. Shen, K. Jia, T. Bing, Z. Zhang, X. Zhen, X. Liu, N. Zhang and D. Shangguan, *Anal. Chem.*, 2020, **92**, 5370–5378.
28 Y. Zhu, Z. Xu, J. Gao, W. Ji and J. Zhang, *Biosens. Bioelectron.*, 2020, **160**, 112210.
29 S. Arshavsky-Graham, K. Urmann, R. Salama, N. Massad-Ivanir, J. G. Walter, T. Scheper and E. Segal, *Analyst*, 2020, **145**, 4991–5003.
30 Z. Liu, S. Lei, L. Zou, G. Li, L. Xu and B. Ye, *Biosens. Bioelectron.*, 2019, **131**, 113–118.
31 M. Anjomshoa and M. Torkzadeh-Mahani, *J. Fluoresc.*, 2016, **26**, 1505–1510.
32 F. A. P. Crisafuli, E. B. Ramos and M. S. Rocha, *Eur. Biophys. J.*, 2015, **44**, 1–7.
33 J. Q. Chen, S. F. Xue, Z. H. Chen, S. Zhang, G. Shi and M. Zhang, *Biosens. Bioelectron.*, 2018, **100**, 526–532.
34 N. Cheng, D. Du, X. Wang, D. Liu, W. Xu, Y. Luo and Y. Lin, *Trends Biotechnol.*, 2019, **37**, 1236–1254.
35 D. Daassi, K. M. Mahoney and G. J. Freeman, *Nat. Rev. Immunol.*, 2020, **20**, 209–215.
36 G. Chen, A. C. Huang, W. Zhang, G. Zhang, M. Wu, W. Xu, Z. Yu, J. Yang, B. Wang, H. Sun, H. Xia, Q. Man, W. Zhong, L. F. Antelo, B. Wu, X. Xiong, X. Liu, L. Guan, T. Li, S. Liu, R. Yang, Y. Lu, L. Dong, S. McGettigan, R. Somasundaram, R. Radhakrishnan, G. Mills, Y. Lu, J. Kim, Y. H. Chen, H. Dong, Y. Zhao, G. C. Karakousis, T. C. Mitchell, L. M. Schuchter, M. Herlyn, E. J. Wherry, X. Xu and W. Guo, *Nature*, 2018, **560**, 382–386.